Crystallinity and size control of colloidal germanium nanoparticles from organogermanium halide reagents.

Bruno Pescara,[1,2,3] Klaus Lips,[1,2,4] Simone Raoux,[1,2,5] Katherine A. Mazzio[1,2,*]

[1]Institute for Nanospectroscopy, Helmholtz-Zentrum Berlin für Materialien und Energie GmbH, Albert-Einstein-Straße 15, 12489 Berlin, Germany

[2]Energy Materials In-Situ Laboratory Berlin (EMIL), Helmholtz-Zentrum Berlin für Materialien und Energie GmbH, Albert-Einstein-Straße 15, 12489 Berlin, Germany

[3]Department of Chemistry, Humboldt-Universität zu Berlin, Brook-Taylor-Straße 2, 12489 Berlin, Germany

[4]Department of Physics, Freie Universität Berlin, Arnimallee 14, 14195 Berlin, Germany

[5]Department of Physics, Humboldt-Universität zu Berlin, Newtonstraße 15, 12489 Berlin, Germany

KEYWORDS Nanoparticles, Amorphous, Crystalline, Germanium, Sulfur, Colloidal synthesis.

ABSTRACT: Germanium (Ge) nanoparticles (NPs) are gaining increasing interest due to their properties that arise in the quantum confinement regime, such as the development of the band structure with changing size. While promising materials, significant challenges still exist related to the development of synthetic schemes allowing for good control over size and morphology in a single step. Herein, we investigate a synthetic method that combines sulfur and primary amines to promote the reduction of organometallic Ge(IV) precursors to form Ge nanoparticles at relatively low temperatures (300°C). We propose a reaction mechanism and examine the effects of solvents, sulfur concentration, and organogermanium halide precursors. Hydrosulfuric acid (H_2S) produced *in-situ* acts as the primary reducing species, and we were able to increase the particle size more than two-fold, both by tuning the reaction time and quantity of sulfur added during the synthesis. We found that we are able to control the crystalline or amorphous nature of the resulting nanoparticles by choosing different solvents and propose a mechanism for this interaction. The reaction mechanism presented provides insight into how one can control the resulting particle size, crystallinity, and reaction kinetics. While we demonstrated the synthesis of Ge nanoparticles, this method can potentially be extended to other members of the group IV family.

Introduction:

Group IV semiconducting materials, such as silicon (Si) and Ge, are good examples for observing and investigating the size-dependent properties that arise due to quantum confinement.[1–6] In their bulk form, group IV materials have an indirect band gap, but quantum confinement induces electronic perturbations that force the system to exhibit direct band gap transitions, resulting in excitons displaying optical transitions in the visible spectral region.[2,7–10] The favorable electronic properties and narrow band gap of bulk Ge (0.67 eV at a temperature of 300 K),[11] coupled with its large Bohr radius ($a_0 \approx 24$ nm)[12,13] renders quantum confinement effects observable at relatively large particle sizes. This allows exploitation of the effects arising due to quantum confinement, such as decoupling the thermal and electrical conductivity[14–16] or tuning light emission[17–19] at relatively large sizes, making Ge nanoparticles particularly attractive for many applications, such as bio-imaging and thermoelectric devices, among others.[20–23]

Despite their great promise, there are still several scientific challenges that need to be addressed before taking advantage of group IV nanoparticles in new technologies. One key issue revolves around finding a synthetic route for these nanomaterials that provides good control over size and morphology, while simultaneously being scalable, cost-effective, and environmentally friendly. To this end, solution-based colloidal syntheses can offer several advantages relative to other methods. Ge, however, has proven challenging to synthesize colloidally, which has been largely attributed to its redox potential ($Ge^{+4} + 4e^- \rightarrow Ge^0$ requires +0.12 V).[11] Such a redox potential makes the utilization of either high temperatures or strong reducing agents, popular choices to form Ge^0.[10,24–32] These strong conditions generally make good control over size and crystallinity in one step difficult to achieve.[33,34]

Ge NPs have previously been synthesized using a variety of precursors.[10] Among the most common are Ge halides, including $GeCl_4$,[26,35–38] GeI_4,[27,35] and GeI_2,[27,28] as well as organogermanium precursors such as tetraethyl germane (TEG),[29] diethyl germane (DEG),[29–31] and $Ge[N(SiMe_3)_2]_2$.[32] Due to the relatively low boiling point of Ge(IV) chlorides and bromides (*i.e.* the boiling point of $GeCl_4$ is 86.55 °C),[11] their reduction reactions are limited to low temperatures. This results in the requirement of using highly reactive reducing agents, among which metallic Na,[38] NaK alloys,[26,38] $NaBH_4$,[39] and $LiAlH_4$[35] have been used. Utilizing common hydride reducing agents, such as $LiAlH_4$, for the reduction of Ge halides also poses hazards related to the formation of GeH_4 as a byproduct, which is an extremely reactive and highly pyrophoric gas. Along with safety concerns, the development of GeH_4 gas as a by-product results in a significant loss of the Ge present,[12,27] limiting the chemical yield of these synthetic methods. For TEG, DEG, and

$Ge[N(SiMe_3)_2]_2$ precursors, thermal reduction was previously used to prepare Ge nanocrystals at elevated temperatures higher than 300 °C.[29,30,32] Reactions involving TEG and DEG were typically performed in supercritical solvents, well beyond the range suitable for simple bench-top experiments.[30] Most of the aforementioned studies successfully achieve some properties such as low temperature, standard benchtop chemistry, and the use of mostly benign reagents. Nevertheless, most often synthesis performed in presence of strong reducing agents or thermal decomposition are chosen, here we attempt to show a synthetic route which specifically not adopt a strong reducing agent as reagent.

Warner described a colloidal synthesis in which Sulfur (S) is used to promote the formation of Ge nanocrystals from an organometallic precursor, triphenylgermanium chloride, at a low temperature (300 °C) using the primary amines oleylamine (OAm) or hexadecylamine (HDA) interchangeably.[40] This method has the advantages of utilizing benign reagents, relatively low temperatures, and standard benchtop chemistry. We intended to use a modified version of this synthetic method as a springboard for the realization of Ge NPs with controlled properties.

We investigate the synthesis of Ge nanoparticles from a variety of organogermanium halide precursors in the presence of different quantities of S and a variety of solvent/capping agents. While S and oleylamine have been used in tandem extensively in nanoparticle synthesis,[41–43] we build upon an understanding of the underlying reaction mechanism through identification of the reducing agent, understanding its interaction with the metallic precursor, and determining how the concentration and composition of the reaction monomers affect the resulting product. Hard-soft acid-base chemistry is used to predict the reactivity of different organogermanium halides, and their effects on the reaction kinetics. Ultraviolet-visible (UV-Vis) spectroscopy measurements have been used to follow the growth dynamics and the optical properties of the products, while the morphology of the NPs has been investigated through a series of characterization techniques, including Raman spectroscopy, transmission electron microscopy (TEM), and X-ray diffraction (XRD). Ultimately, we are able to propose a general reaction mechanism that we manipulate towards control over crystalline or amorphous morphology alongside size tunability for our Ge NPs.

Experimental Methods:

All syntheses were carried out in the chemistry laboratory at the Energy Materials *In-situ* Laboratory Berlin (EMIL), jointly operated by Helmholtz-Zentrum Berlin für Materialien und Energie, GmbH (HZB) and the Max-Planck Society (MPG). All materials were used as received unless otherwise noted. Diphenyl germanium dichloride (Ph_2GeCl_2) 95%, sulfur (S) ≥ 99.5%, oleylamine (OAm) 98%, hexadecylamine (HDA) 98%, toluene (Tol) ≥ 99.5%, chloroform ($CHCl_3$) 98%, and methanol (MeOH) ≥ 99.8% were purchased from Sigma Aldrich. Triphenylgermanium chloride (Ph_3GeCl) 99% was obtained from either Sigma Aldrich or Santa Cruz. Triphenylgermanium bromide (Ph_3GeBr) 95%, was procured from ABCR.

Synthesis:

All syntheses were conducted under N_2 atmosphere using standard Schlenk techniques. For all synthetic procedures, the chosen capping agent also acted as the primary solvating species. Throughout this study, the molar ratio between the Ge precursor of interest and the different capping agents was kept constant at [Ge:capping agent] = 1:125. The concentration of S, in the sulfur precursor was chosen such that once the two precursors were added together, the final total Ge to S molar ratio, [Ge:S], was 1:0.25, 1:0.5, 1:1, or 1:2 as intended.

Germanium precursor preparation (1): A 100 mL three neck round bottom flask was charged with a mixture of 5.89×10^{-4} mol of organogermanium halide precursor and 4.48×10^{-2} mol of the desired solvent/capping agent (OAm, or HDA as appropriate). This solution was then heated to 120 °C and allowed to stir under nitrogen atmosphere for 30 minutes.

Nuclear Magnetic Resonance (NMR) peak assignments for *1* with Ph_3GeCl and OAm:

^{1}H-NMR($CDCl_3$ δ 7.26, 500 MHz) *o*-Ar-**H** δ 7.63-7.61 ppm (m), *m*-Ar-**H** δ 7.46-7.40 ppm (m), *p*-Ar-**H** δ 7.35-7.31 ppm (t) **H**C=C**H** δ 5.34 ppm (t), R-C**H₂**-N δ 2.67 ppm (t), C=C-C**H₂** δ 2.00 ppm (q), R-C**H₂**-C-N δ 1.42 ppm (quint), R-(C**H₂**)n-R δ 1.38-1.23 ppm (m), R-N**H₂** δ 1.22 ppm (s), R-C**H₃** δ 0.87 ppm (t).

^{13}C-NMR($CDCl_3$ δ 77.16, 500 MHz) **C**=**C** δ 130 ppm, R-**C**-N δ 42.42, R-**C**-C-N δ 34.05 ppm, **C**-C=C-**C** δ 27.32-27.02 ppm, C-**C**-R δ 22.79, **C**-R δ 14.20 ppm.

Sulfur precursor preparation (2): In a separate 100 mL two neck round bottom flask equipped with septa, a condenser, and a stir bar, a mixture of S (between 1.56×10^{-4} and 1.25×10^{-3} depending on the chosen [Ge:S]) and 3×10^{-2} of the same solvent/capping agent used for the production of *1* (OAm, or HDA as appropriate) was loaded. This solution was then heated to 180 °C and allowed to stir for 20 minutes under N_2.

NMR peak assignments for *2* with S and OAm:

^{1}H-NMR($CDCl_3$ δ 7.26, 500 MHz) **H**C=C**H** δ 5.35 ppm (t), R-C**H₂**-N δ 2.67 ppm (t), C=C-C**H₂** δ 2.01 ppm (q), R-C**H₂**-C-N δ 1.42 ppm (quint), R-(**CH₂**)$_n$-R δ 1.38-1.22 ppm (m), R-N**H₂** δ 1.01 (broad), R-C**H₃** δ 0.88 ppm (t).

^{13}C-NMR($CDCl_3$ δ 77.16, 500 MHz) **C**=**C** δ 130 ppm, R-**C**-N δ 42.42, R-**C**-C-N δ 34.05 ppm, **C**-C=C-**C** δ 27.32-27.02 ppm, C-**C**-R δ 22.79, **C**-R δ 14.20 ppm.

Nanoparticle synthesis: the temperature of *1* was raised to 280 °C. Once this temperature was reached, *2* was then quickly injected using a glass syringe, with a subsequent drop in the vessel temperature of approximately 50 °C. The temperature set point was increased to 300 °C before the re-establishment of thermal equilibrium and kept constant at this temperature for 1 hour to allow the components to react. The development of a dark ring above the surface of the slurry was typically observed prior to a color change in the bulk of the solution. After the desired reaction time, the final reaction slurry was air cooled to room temperature prior to purification. Slurry aliquots of about 3.5 mL were transferred to 15 mL centrifuge tubes and dispersed with methanol, stirred vigorously, and subsequently sonicated for a few minutes to ensure good dispersion of the products prior to centrifuging at 9000 rpm for 15 minutes. After centrifugation, the supernatant was discarded, the precipitate was dispersed in toluene or chloroform, and the purification process was repeated under the same conditions. For the final step of the purification process, the precipitate was dispersed in $CHCl_3$ and centrifuged as before, and, if needed, repeated until the supernatant was clear. The particles were finally dispersed in ≈ 3 mL of $CHCl_3$ in order to transfer to storage vials, and then

dried on a rotary evaporator at 40 mbar and 45 °C. The dried materials were stored in a glove box under N_2 atmosphere.

Yield calculation, the obtained dried product has been weighted. In order to determine the organic fraction of the obtained product an aliquot of the dried product has been used for a Thermogravimetric analysis (TGA). The measure has been carried from 20° to 900°C with a heating ramp of 20°C/min, followed by an isothermal for 10 min. the whole measurement has bed executed under flowing nitrogen about 40 ml/min. The TGA profile shows a mass loss up to 90%, as shown in Figure S1 in supporting information. The residual mass has been considered to be 100% Ge. This weight has been converted into mole and used to calculate the yield. For the syntheses conducted with Ph_3GeCl in a ratio of [Ge:S] 1:1 for OAm and HDA were 83% and 86%, respectively.

NMR peak assignments for the crude product from the synthesis conducted with Ph_3GeCl, S, and OAm:

^{1}H-NMR($CDCl_3$ δ 7.26, 500 MHz) S-Aryl-**H** δ 7.24-7.13 ppm (m), **H**C=C**H** δ 5.34 ppm (t), S-**H** δ 3.40 ppm (s), **H**-(C=S)-N δ 3.33 ppm(t), R-(C**H₂**)₂-S δ 2.58 (m), R-C**H₂**-N δ 2.22 ppm (t), C=C-C**H₂** δ 2.01 ppm (m), R-C**H₂**-C-N δ 1.64 ppm (m), R-(C**H₂**)$_n$-R δ 1.61-1.40 ppm (m), R-C**H₃** δ 0.88 ppm (t).

Characterization:

A Bruker AVANCE III 500 MHz NMR spectrometer was used to record ^{1}H and ^{13}C NMR spectra at the Core Facility BioSupraMol at the Freie Universität Berlin. For all NMR spectra, $CDCl_3$ was used as solvent, with $CHCl_3$ used as an internal standard.

Transmission electron microscopy (TEM) was carried out at the Bundesanstalt für Materialforschung und -prüfung (BAM) in the structure analysis division. Measurements were performed on a Thermo Scientific Talos Arctica 200 kV FEG TEM. All TEM samples were prepared by drop casting NP dispersions in chloroform on 200 mesh copper TEM grids coated with ultrathin carbon and lacey carbon support films (PLANO, GmbH). All TEM data analysis was carried out using ImageJ software.[44]

Raman measurements were carried out with a Micro-Raman system LabRam from Dilor with an excitation wavelength of 632.8 nm from a He-Ne laser (laser energy 700 or 70 µW depending on the application of different filters). Raman samples were prepared by drop casting concentrated NP dispersions in toluene onto clean microscope slides.

UV-Vis measurements were carried out in the characterization lab (SCALA) at EMIL, using an Ocean Optics DH-mini benchtop spectrometer with a deuterium and halogen light sources, equipped with a USB4000-XR1-ES detector. All samples were prepared from dilute solutions in toluene, with measurements performed in quartz cuvettes.

XRD measurements were carried out in the X-Ray CoreLab at HZB on a Bruker D8 X-ray powder diffractometer (XRD) in Bragg-Brentano geometry, equipped with a LynxEye detector, and using Cu K-α_{1+2} radiation. All data have been analyzed with DiffracEVA software using the ICDD PDF4+ database.

TGA measurement were carried out in the in the characterization lab (SCALA) at EMIL, using a TGA Q500 and platinum pans from TA instruments.

Results and discussion:

We first investigated systems with OAm as solvent and different [Ge:S], namely 1:2, 1:1, and 1:0.5. This was done in order to assess the effect of the reducing agent concentration on the size of the resulting particles. In our case, the S quantity is related to the population and production rate of the reducing agent. According to classical nucleation theory (CNT), we expected to observe an inverse relationship between the particle size and the amount of reducing species.[45–47]

We used TEM to analyze the morphology of our products, which can be found in Figure 1 a, b and c. The average diameters for each product, along with the resulting morphology and nucleation time for each synthesis are summarized in Table 1. The results are in line with our expectations from CNT, where the observed average particle size increases with decreasing amount of reducing agent Averages were taken from 150 NPs, obtained via a combination of both high magnification pictures and low magnification overviews, which examples are given in Figure S2 in Supporting Information. A complete size distributions are given in Figure S3 in the Supporting Information. We found that the majority of nanoparticles produced were amorphous, in contrast to the expected crystalline morphology. A first indication of this can be seen in the insets of Figure 1 a, b and c, where Fast Fourier Transforms (FFTs) of each respective TEM image are shown. The FFTs show diffuse ring patterns, which are characteristic of amorphous materials. The amorphousness is also supported by the corresponding XRD patterns provided in Figure 2a. We did find some contribution from crystalline particles in the [Ge:S] 1:0.5 sample, shown in Figure 1a, where the FFT clearly demonstrates crystalline diffraction signals. The crystal lattice fringes show a lattice constant of 3.2 Å, which is coherent with the (111) spacing of the cubic Ge lattice.[13,27]

From the literature, we had expected the formation of primarily crystalline products when using OAm as solvent.[40] We attribute this discrepancy to differences in the

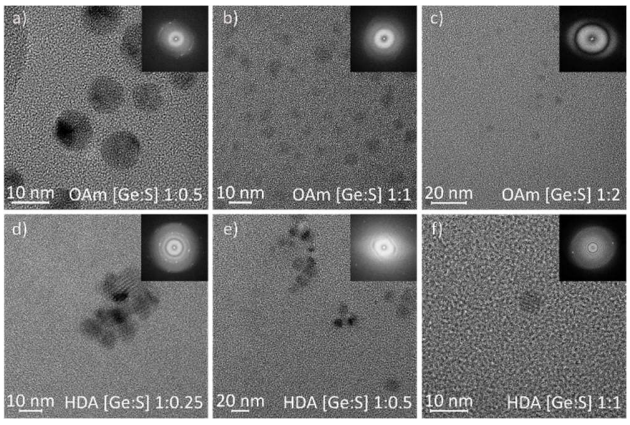

Figure 1: TEM images of the worked up product from a) OAm [Ge:S] 1:0.5, b) OAm [Ge:S] 1:1, c) OAm [Ge:S] 1:2, d) HDA [Ge:S] 1:0.25, e) HDA [Ge:S] 1:0.5, and f) HDA [Ge:S] 1:1 syntheses. The inset in each image is an FFT of the corresponding whole image.

Table 1: Summary of the data collected for all the syntheses

Solvent	[Ge:S]	t_{nucl} (min)	TEM Diamter (nm)	Scherrer eqn. Diameter (nm)	Morphology
OAm	1:0.5	10	8.2 ± 4.5	-	Amorphous (small crystalline fraction)
OAm	1:1	14	4.6 ± 2.6	-	Amorphous
OAm	1:2	21	3.5 ± 1.9	-	Amorphous
HDA	1:0.25	19	12.2 ± 3.2	15.9	Crystalline
HDA	1:0.5	7	8.4 ± 1.7	9.1	Crystalline
HDA	1:1	4	6.8 ± 2	7	Crystalline

observed nucleation times (t_{nucl}). We used UV-Vis spectroscopy to monitor the t_{nucl} for each reaction by taking aliquots at different times. At the time of nucleation, a small shoulder would develop in the spectra, which we could clearly identify in the derivative spectrum. An example of this analysis is given in Figure S4 of the Supporting Information. We expected the development of an absorption edge feature at longer wavelength, as predicted by the Brus equation and the effective mass approximation, but we were unable to observe it. We assume the lack of this feature is due to a screening effect arising from the large absorbance cross section of the residual polymer ligand, which renders the feature indistinguishable from background noise. We found significantly longer t_{nucl} for all samples synthesized with OAm as the solvent than the immediate nucleation that was expected from the literature.[40] We found that for syntheses with OAm, there is a delay in t_{nucl} with increasing sulfur concentration; this is surprising because these are not in line with what one would expect from CNT. One explanation for this behavior could relate to a decrease in the diffusion rate of the reduced species in solution as the S concentration increases. A significant reduction in the diffusion rate would affect the rate of nucleation, which could simultaneously delay and hinder the development of the thermodynamically stable crystalline morphology, in addition to hindering NP growth, thereby producing smaller NPs. Because the amorphous phase is not the most thermodynamically stable structure of Ge, its development indicates in a kinetically driven process. Since the particles reported herein had a shorter growth period (defined as total reaction time, minus t_{nucl}), we could expect this to not only affect the size of the product, but also its crystallinity. Such behavior can be observed in the product of [Ge:S] 1:0.5, which had the lowest sulfur concentration, and is the only sample that exhibits the presence of some larger partially crystalline particles.

We hypothesize that as the particles nucleate, due to the presence of sulfur, predominantly kinetic dynamics produce the amorphous products. The geometrical frustration due to their high curvature at small size prevents the formation of a crystal structure, resulting in an amorphous nanoparticle where the frustration is relaxed through isolated defects.[48] As the particle grows, the most stable thermodynamic morphology starts to develop. The volume and surface area both increase, resulting in a decrease of the curvature of the particle, and an accumulation of topological defects. Eventually, a critical threshold will be reached, and further relaxation will take place involving a mechanism of crystal formation and defect annihilation.[48,49]

We later performed syntheses with HDA as the solvent. HDA is similar to OAm, where both solvents have a long alkyl chain that is terminated by a primary amine group, but HDA is saturated, whereas OAm has a single double bond. These long-chain primary amines are often used interchangeably in NP synthesis due to their similar properties, including their relatively high boiling points. Because of the similarities in these solvents, we expected a similar morphology to result.

For the syntheses conducted in HDA, we investigated a [Ge:S] of 1:0.25, 1:0.5, and 1:1. The products of the HDA syntheses were similarly characterized using TEM and XRD, as shown in Figure 1 d, e and f and Figure 2 b, respectively, and summarized in Table 1. These results show that the particles formed in HDA exhibit larger particle sizes and completely

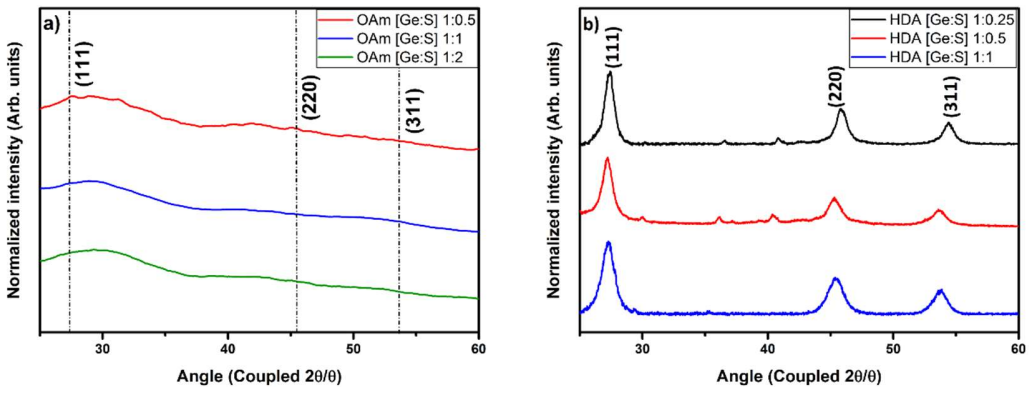

Figure 2: XRD diffractograms for samples synthetized with different [Ge:S] molar ratios in a) OAm, and b) HDA. The dash dot lines are the expected position of the Bragg peaks, whit the respective Miller indexes.

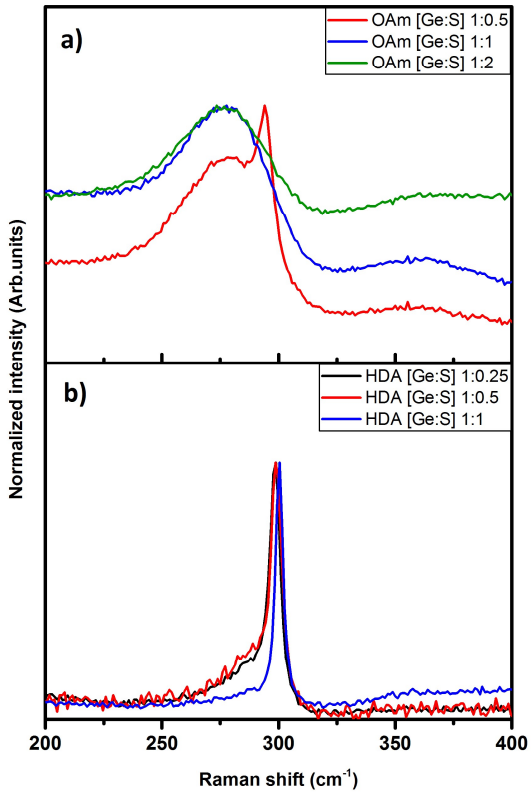

Figure 3: Overlay of normalized Raman spectra for samples synthetized with different [Ge:S] molar ratios in a) OAm, and b) HDA.

crystalline morphology instead of primarily amorphous particles observed for syntheses in OAm. The diameter of the particle produced with HDA, thanks to the presence of the diffraction pattern, has been determined via the Scherrer equation using the dominant peak of the diffractogram, namely the (111) diffraction signal. The crystalline products showed a face-centered cubic diamond crystal structure, with a coherent lattice constant of 3.2 Å, as calculated from the (111) diffraction signal in the XRD pattern in Figure 2b, in Figure S5 a scale up of Figure 1 f and the edge of a NPs cluster are shown, to highlight the presence of crystalline fringes. The t_{nucl} observed in HDA are shorter in comparison with OAm, and they decrease as the sulfur concentration increases, as expected from CNT. This results, in particular the presence of a mixed amorphous and crystalline phase in the sample with [Ge:S] 1:0.5, similar to the results showed by Bernard *et. al.*,[28] points toward a non-trivial effect of the solvents on growth and crystallinity of germanium NPs.

Syntheses with HDA and [Ge:S] > 1:1 have been attempted, with immediate nucleation observed, but no nanoparticles could be recovered during the work up. This could result from the nuclei that are formed being too small to be stable in solution, or because the nanoparticles were too small to be isolated through centrifugation.

To confirm the successful reduction of the organogermanium halide precursors into Ge^0 species and its crystalline or amorphous morphology, Raman spectroscopy was carried out. We observed the presence of covalent Ge-Ge bonds, as shown in Figure 3 a and b. Each of the samples produced with OAm has a wide resonance feature centered at 275 cm^{-1}, which is typical of bonding modes for amorphous Ge.[50] The [Ge:S] 1:0.5 sample also shows a small sharp feature centered at 295 cm^{-1}, which is due to the covalent bond in crystalline Ge,[51] and acts as cross-confirmation of the nature of the lattice fringes observed in the TEM images. The products synthesized using HDA clearly show crystalline features centered at 300 cm^{-1}, as expected from purely crystalline Ge-Ge bonds. We attribute the small shift of the position of the crystalline peaks in the OAm product to the difference in size of the corresponding products and the interaction of the crystallite in the OAm [Ge:S] 1:0.5 product with the amorphous phase in which it is embedded.[52] The small anisotropy of the peaks observed in the products formed with HDA, was be attributed to a minor fraction of amorphous phase.

Covalent interactions between Ge and S or nitrogen are strongly Raman active, making Raman a good method for exploring the development of any secondary phases under our reaction conditions We would expect many strong and relevant features associated with Ge-S or Ge-N Raman active modes to show up in the regions between 200 and 1100 cm^{-1}.[53–55]. In Figure 3 a and b we do not observe any indication of these secondary species, but we carried out measurements at higher Raman shifts in order to further demonstrate that no secondary Ge species formed during synthesis. These results are presented in Figure S6 of the Supporting Information. We did not observe any relevant features, indicating that our NP products are composed solely of amorphous or crystalline elemental germanium. This observation is also supported by the XRD measurements, where no evidence of signals associated with GeS are found.

Reaction mechanism:

In an effort to explain the development of the different morphologies in our nanoparticle products from mostly similar species, we investigated the reaction mechanism via ^{1}H NMR spectroscopy, and confirmed the peak assignments via heteronuclear multiple quantum coherence correlation spectra (^{1}H ^{13}C-NMR-HMQC), the results of which can be found in Figure 4 and Figure S7 of the Supporting Information, respectively. Through analyzing these spectra and in conjunction with the literature, we are able to support the reaction mechanism outlined in Scheme 1, and propose the mechanism in Scheme 2. In Figure 4, we present ^{1}H NMR spectra for pure OAm as reference, the sulfur precursor outlined in *2*, and the crude reaction slurry prior to purification. For neat OAm, the N-H proton is located at δ 1.20 ppm. An upfield shift of this proton is observed when OAm is in the presence of S, both in the sulfur precursor (to δ 1.09 ppm) and in the reaction crude (to δ 1.11 ppm), as indicated by the shift of the black solid square in Figure 4. This is in coherence with the literature, and is ascribed to the interaction between the amino group and S, where the nitrogen of the amine induces an opening of the S_8 ring via nucleophilic attack, resulting in the formation of alkyl ammonium poly-sulfides at room temperature, as described in Scheme 1 Reaction 2.[56] Upon heating, the polysulfide ions can react with excess alkyl amine to liberate H_2S according to a variety of progressive condensation reactions (Scheme 1 Reaction 4-6). By placing a piece of PbO coated paper within the reaction vessel and observing its transformation to PbS by a color change from yellow to black (Figure S8 in the Supporting Information), we found that these subsequent condensation reactions occur above approximately 100 °C. Control syntheses were also performed that demonstrate

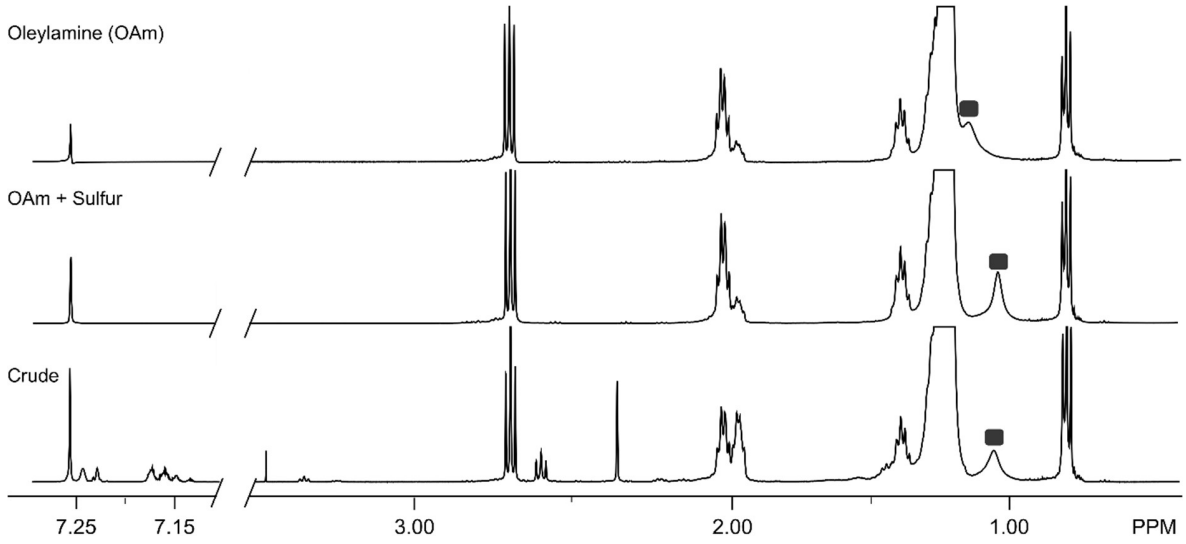

Figure 4: ^{1}H-NMR spectra of (top) pure oleylamine, (middle) the product of **2** (OAm after S addition), and (bottom) the reaction slurry prior to purification. The small black box highlights changes in the N-H chemical shift. The feature at δ 1.95 ppm is related to the thioaminoamide, the small triplet at δ 2.58 ppm is related to the production of the r-poly-OLA. A new triplet at δ 3.33 ppm, corresponds to the α-carbon of a thioamide, while the other singlet at δ 3.40 ppm arise from S-H modes

that the production of H_2S continues for longer than 2 hours and 30 minutes under our reaction conditions.

The reactions outlined in Scheme 1 Reactions 1-2 and 4-6 are expected to occur regardless of the aliphatic amine used during synthesis. However, since we observed differences in the products between OAm and HDA, it is of particular importance to understand the interaction mechanism between S and unsaturated monomers, as in OAm. The relevant process is known as vulcanization, which is preceded by the formation of linear di-radicals from the homolytic breakup of labile S-S bonds.[57,58] These sulfur radicals are known for having a high affinity towards double bonds, and because oleylamine possesses a long alkyl chain with an unsaturated double bond, the oleylamine and S species can undergo a radical polymerization. This results in the sulfur di-radicals establishing bridges between oleylamine molecules and cross-linking them, forming what is called a poly-(oleylamine-random-sulfur) copolymer, or poly-OLA-r-S, as shown in Scheme 1 Reaction 3.[59] This product can be observed in the reaction crude by the development of a signal related to the sulfur precursor and neat OAm. The multiplet at δ 2.58 ppm corresponds to the expected signal for protons in positions α to a C-S bond, which is in accordance with the production of the r-poly-OLA polymer. A small analog multiplet centered at δ 2.56 ppm can be found in the NMR spectrum of the sulfur precursor *2* as shown in Figure S9. Due to the lower temperature at which this solution is prepared, together with the four time shorter reaction time, the intensity of the feature is so low to make it almost indistinguishable from the background.

Scheme 1: Reaction (1). Temperature induced homolytic breakup of the S-S bond. Reaction (2). Ring opening and nucleophilic attack by the nitrogen to the S_8 ring. Reaction (3). Radical polymerization of S and an unsaturated aliphatic chain. Reaction (4). Thioamide formation. Reaction (5) and (6) subsequent condensation reactions.

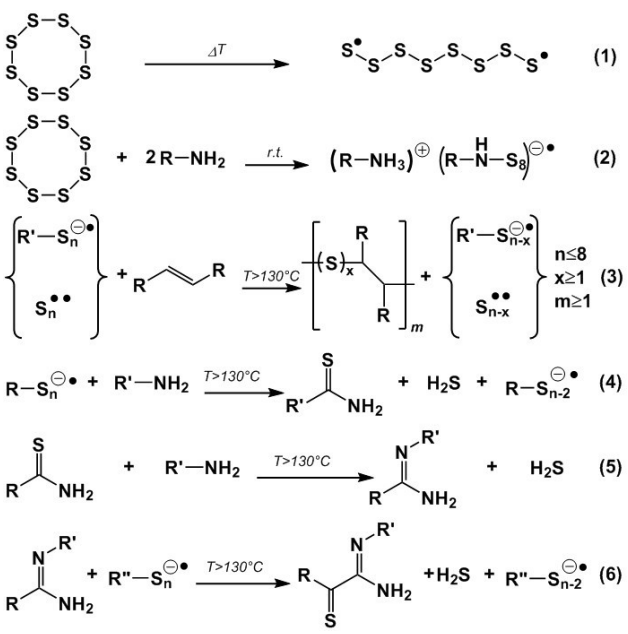

Scheme 2: Reaction (1). Cleavage of the halogen and amine coordination. Reaction (2). Reduction of Ge^{4+} to Ge^{2+} by H_2S; thiophenol is formed as a by-product. Reaction (3). Spontaneous disproportionation of Ge^{2+} over 140 °C to Ge^{0} and Ge^{4+}.

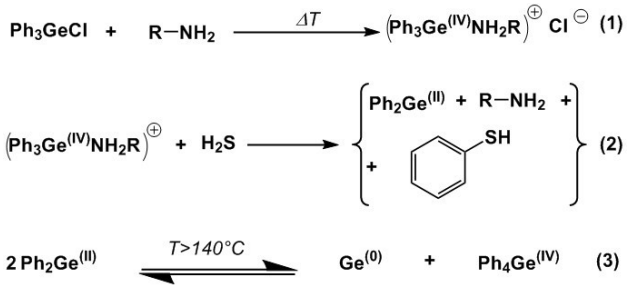

The formation of the poly-OLA-r-S supports our initial hypothesis, where the formation of a polymer hinders the diffusion of the reduced Ge^0 species to the Ge nuclei. This product cannot develop with HDA as a precursor, due to the lack of unsaturated bonds.

After elucidation of the reducing agent and its observed production, we were able to propose a general reaction mechanism for the reduction process that forms Ge nanoparticles from an organogermanium chloride precursor, as outlined in Scheme 2. In Scheme 2 Reaction 1, the cleavage of the chloride leaving group is demonstrated. Given the presence of a Lewis base as solvent, the amine can interact with the metallic center via its lone pairs, which facilitates this halogen cleavage process. We hypothesize that the spontaneous cleavage of the halogen precedes the interaction of the Lewis base with the metal center, due to the coordination sphere of the Ge(IV) containing only four positions.[60] Scheme 2 Reaction2 shows the reduction of Ge^{4+} to Ge^{2+}. After halogen cleavage, the stabilized Ge(IV) species interacts with the H_2S. Due to the electron configuration of the H_2S and the steric hindrance of species coordinating to Ge, it is most likely that the H_2S interacts with one of the phenyl groups, which are rendered more electrophilic from bonding with Ge. We presume that the germanium central atom, particularly if still directly bound with the halogen, acts as an electron withdrawing group (EWG) activating the meta position of the phenyl groups for an electrophilic substitution. Such atomic structure can activate the aromatic rings for an aromatic substitution reaction. The S attacks the phenyl rings, triggering an electronic rearrangement, which leads to the reduction of the central germanium. This thereby reduces the Ge only from +4 to +2; this is supported by the observation that thiophenol is produced as a reaction byproduct. The singlet at δ 3.40 ppm in Figure 4 can be assigned to the chemical shift of the proton from the S-H bond in a thiophenol molecule. In Scheme 2 Reaction 3, the disproportionation reaction of Ge^{2+} to Ge^0 and Ge^{4+} is shown. The spontaneous disproportionation of Ge^{2+} to Ge^0 and Ge^{4+} is well known in the literature, and has been reported as a critical step for the production of Ge^0; it is known to occur at temperatures greater than 140 °C.[4,12,27,61,62] The disproportionation reaction is the final step of the reduction mechanism, and it is important to notice that the Ge(IV) species created during this process can potentially re-enter the reaction mechanism in Scheme 2 Reaction 2, but with different kinetics.[4] This mechanism is supported by observed yields in excess of 83%, which is substantially greater than the otherwise theoretical limit of 50% imposed by the disproportionation reaction. In addition, we were able to exclude direct thermal decomposition as the route from Ge^{4+} to Ge^0 by performing a series of syntheses under the same conditions, but excluding S from the reaction. During the thermal decomposition experiments, we found no indication of Ge^0 production, even after extending the reaction time by 50%, or to 1.5 hours.

The elucidation of the reaction mechanism, in particular understanding variables such as the reducing agent and its production, its interaction with the Ge precursor material, and the polymerization process of the amine and their role in precursor stabilization provides us with a parameter toolbox with which to control the dynamics and kinetics of this system. In particular, the confirmation of formation of the r-poly-OLA polymer presents a means for explaining the differences observed in the products formed with the amines that are typically used interchangeably in NP synthesis.

We hypothesize that the discrepancy in behavior between the syntheses performed in OAm and HDA is related to the formation of the r-poly-OLA polymer, which is absent from HDA (Scheme 1 Reaction 3). This ultimately affects the diffusion rate of reduced species to the NP nuclei. This is demonstrated by the opposite trend of the t_{nucl} with increasing sulfur, where nucleation is delayed when synthesized in OAm (in opposition with CNT), while it is faster when synthesized in HDA (in agreement with CNT). Such an effect not only has an impact on the particle size, but can also alter the relationship between thermodynamic and kinetic parameters. The Gibbs free energy for nucleation (ΔG*) can be defined as:

$$\Delta G^* = \left(\frac{16\pi}{3}\right)\gamma^3/(\rho|\Delta\mu|)^2$$

where γ is the surface free energy, ρ is the number density of the crystal phase, and Δμ is the difference of chemical potential between the solid and liquid phases, which increases with increasing supersturation.[63] The rate of nucleation can be expressed in an Arrhenius type equation as:

$$I = \kappa e^{(-\Delta G^*/kT)}$$

where κ is a numerical kinetic prefactor, k is Boltzmann's constant, and T is the absolute temperature.[63]

In CNT, the interrelationship between γ, and Δμ are generally neglected, resulting in the energy barrier always decreasing with increasing supersaturation. This has been shown to not hold for large supersaturation.[63] The formation of a polymer resulting from the cross linking of S with the unsaturated bond in OAm will affect the rheological properties of the solution, slowing down the diffusion of reduced monomers, and decreasing the prefactor κ,[63] furthermore, recent works indicates that polydispersity can greatly affect the nucleation rate based on a development in the crystal-fluid interface free energy.[64] Given the similarity between the two solvents examined (OAm and HDA), and the following similarity in thermodynamics for both, the observed difference in crystallinity must be due to changes in the kinetic factors arising from the polymer formation, favoring the crystalline thermodynamic product for the HDA syntheses, as opposed to the kinetically favored amorphous phase for OAm.

Organogermanium halide precursor:

The importance played by the organogermanium halide precursor in the kinetics of the synthesis was also investigated. Properties such as the ligand binding characteristics of a metallic precursor can have dramatic effects on the kinetics of reduction. Drastic changes in reaction time, reaction temperature, final morphology, and solubility in the solvent can occur depending on the ligand properties. According to the Lewis Hard Soft Acid Base (HSAB) theory, Ge is considered a hard Lewis acid, chloride is an intermediate base, and bromide is a soft base. It follows that the interaction between Ge and chloride should be stronger relative to the interaction between Ge and bromide, and it should therefore be more difficult to dissociate the hard halogen (chloride). In order to have a better understanding of the role of the organogermanium precursor on the kinetics of the synthesis, three related Ge monomers were investigated: diphenyl germanium dichloride, triphenyl germanium chloride, and triphenyl germanium bromide. All reactions were carried out under similar molar concentrations of Ge precursor to S (or [Ge:S] 1:1). The reaction conducted with triphenyl germanium

chloride at 300 °C showed visible signs of nucleation at 14 minutes, as discussed above. With triphenyl germanium bromide, faster nucleation times were observed, at 10 minutes. When the reaction was performed with diphenyl germanium dichloride at 300 °C, it failed to produce any nanoparticles. When the reaction temperature was raised to reflux, nucleation was eventually observed after approximately 45 minutes, which demonstrates a significant reduction in reactivity relative to the other precursors examined. The substitution of a phenyl group with a chloride in the coordination environment of the Ge precursor results in a shift of the electron density from the metallic center to the new chloride. In terms of HSAB theory, the chloride can be considered a harder base than the aromatic ring due to its higher electronegativity and lower polarizability. The chloride therefore establishes a stronger interaction with the Ge and reduces the reactivity of the dichloride precursor relative to the mono-halogen precursors. The observed differences in t_{nucl} are in line with what is predicted from HSAB theory, and we can arrange the precursors in a reactivity ladder as follows:

$Ph_2GeCl_2 < Ph_3GeCl < Ph_3GeBr$

Given the substantial change in the t_{nucl}, the theoretical relative weakness of the interaction between the bromide and the Ge, and the higher temperature required for reduction of the Ph_2GeCl_2, it follows that the halogen cleavage process outlined in Scheme 2 Reaction 1 is the rate determining step for the reduction. This reactivity ladder can be useful for the extension of this synthetic technique to the synthesis of other group IV compounds.

Conclusions:

In summary, we have investigated the synthesis of Ge NPs from a variety of organometallic Ge precursors with S in different relative molar ratios, and in different primary amines that play a dual role, acting as both the solvents and capping agents. We demonstrated the production of almost completely amorphous NPs when synthesized in OAm, with diameters ranging from 3.5-8.2 nm depending on the concentration of the reducing species. We were able to produce face-centered cubic crystalline NPs when using HDA instead of OAm, with diameters from 7 to 16 nm depending on the sulfur concentration. This demonstrates the possibility to change the crystalline or amorphous nature of the final product based on the solvent used during synthesis. The size and crystallinity of the resulting particles were characterized via TEM, XRD, UV-Vis spectroscopy, and Raman spectroscopy. In an effort to understand the development of the kinetically stabilized or thermodynamic product, we performed NMR spectroscopy to elucidate the reaction mechanism. From these experiments, we were able to identify H_2S as the reducing agent, and detail its interaction with the organometallic precursor. We also investigated the reaction kinetics and assigned the halogen cleavage as the rate-limiting step for NP production. Finally, we were able to produce a reactivity ladder with different substituents in the coordination environment of the Ge precursors as can be understood from HSAB theory.

The synthetic route explored in this contribution allows for control over the size and crystallinity of Ge NPs, and demonstrates that saturated and unsaturated aliphatic amines cannot be used interchangeably as high boiling point solvents. The synthetic methods explored in this study are attractive due to their relatively low-temperature synthesis that uses standard benchtop chemistry techniques and benign reagents. We believe this method can be extended to other members of the group (IV), making this a flexible tool to produce a variety of NPs.

ASSOCIATED CONTENT

Supporting Information. The Supporting Information includes NP size distributions, UV-Vis spectra of time aliquots taken from OAm [Ge:S] 1:0.5, Raman spectra in the range 600-1100 cm^{-1}, ^{1}H ^{13}C-NMR-HMQC spectrum of the reaction slurry of OAm [Ge:S] 1:1, and photos of the PbO coated paper before and after exposure to reaction atmosphere. This material is available free of charge via the Internet at http://pubs.acs.org.

AUTHOR INFORMATION

Corresponding Author

*Email address for K.A.M.: katherine.mazzio@helmholtz-berlin.de.

Author Contributions

The manuscript was written through contributions of all authors. All authors have given approval to the final version of the manuscript.

Notes

The authors declare no conflicts of interest.

ACKNOWLEDGMENT

We would like to acknowledge Dr. Rowan MacQueen for support with UV-Vis Spectroscopy. The authors would also like to acknowledge The Core Facility BioSupraMol of FUB and Dr. Andreas Schäfer for support with their NMR instruments, and the BAM Division 1.3 for structure analysis, in particular Dr. Carsten Prinz and Dr. Franziska Emmerling for access to and support with the TEM.

REFERENCES

(1) Talapin, D. V.; Lee, J. S.; Kovalenko, M. V.; Shevchenko, E. V. Prospects of Colloidal Nanocrystals for Electronic and Optoelectronic Applications. *Chem. Rev.* **2010**, *110* (1), 389–458.

(2) Shiohara, A.; Prabakar, S.; Faramus, A.; Hsu, C.-Y.; Lai, P.-S.; Northcote, P. T.; Tilley, R. D. Sized Controlled Synthesis, Purification, and Cell Studies with Silicon Quantum Dots. *Nanoscale* **2011**, *3* (8), 3364–3370.

(3) Hu, Y.; Churchill, H. O. H.; Reilly, D. J.; Xiang, J.; Lieber, C. M.; Marcus, C. M. A Ge/Si Heterostructure Nanowire-Based Double Quantum Dot with Integrated Charge Sensor. *Nat. Nanotechnol.* **2007**, *2* (10), 622–625.

(4) Lu, X.; De La Mata, M.; Arbiol, J.; Korgel, B. A. Colloidal Silicon-Germanium Nanorod Heterostructures. *Chem. Mater.* **2017**, *29* (22), 9786–9792.

(5) Lu, X.; Adkins, E. R.; He, Y.; Zhong, L.; Luo, L.; Mao, S. X.; Wang, C. M.; Korgel, B. A. Germanium as a Sodium Ion Battery Material: In Situ TEM Reveals Fast Sodiation Kinetics with High Capacity. *Chem. Mater.* **2016**, *28* (4), 1236–1242.

(6) Rabbani, M. G.; Patil, S. R.; Verma, A.; Villarreal, J. E.; Korgel, B. A.; Nekovei, R.; Khader, M. M.; Darling, R. B.; Anantram, M. P. Zero-Bias Photocurrents in Highly-Disordered Networks of Ge and Si Nanowires. *Nanotechnology* **2015**, *27* (4), 045201.

(7) Li, D.; Nielsen, M. H.; Lee, J. R. I.; Frandsen, C.; Banfield, J. F.; De Yoreo, J. J. Direction-Specific Interactions Control Crystal Growth by Oriented Attachment. *Science* **2012**, *336* (6084), 1014–1018.

(8) Kuo, Y. H.; Lee, Y. K.; Ge, Y.; Ren, S.; Roth, J. E.; Kamins, T. I.; Miller, D. A. B.; Harris, J. S. Strong Quantum-Confined Stark Effect in Germanium Quantum-Well Structures on Silicon. *Nature* **2005**, *437*, 1334–1336.

(9) Furey, B. J.; Silbaugh, D. A.; Yu, Y.; Guillaussier, A. C.; Estrada, A. D.; Stevens, C.; Maynard, J. A.; Korgel, B. A.; Downer, M. C. Measurement of Two-Photon Absorption of Silicon Nanocrystals in Colloidal Suspension for Bio-Imaging Applications. *Phys. Status Solidi Basic Res.* **2018**, *255* (4), 1700501.

(10) Carolan, D. Recent Advances in Germanium Nanocrystals: Synthesis, Optical Properties and Applications. *Prog. Mater. Sci.*

2017, *90*, 128–158.

(11) Lide, D. R. *Crc Handbook of Chemistry and Physics a Ready-Reference Book of Chemical and Physical Data Special Student Edition*, 72nd ed.; CRC-press, Ed.; 1993.

(12) Vaughn II, D. D.; Schaak, R. E. Synthesis, Properties and Applications of Colloidal Germanium and Germanium-Based Nanomaterials. *Chem. Soc. Rev.* **2012**, *42* (7), 2861–2879.

(13) Xue, D. J.; Wang, J. J.; Wang, Y. Q.; Xin, S.; Guo, Y. G.; Wan, L. J. Facile Synthesis of Germanium Nanocrystals and Their Application in Organic-Inorganic Hybrid Photodetectors. *Adv. Mater.* **2011**, *23* (32), 3704–3707.

(14) Wang, Z.; Alaniz, J. E.; Jang, W.; Garay, J. E.; Dames, C. Thermal Conductivity of Nanocrystalline Silicon: Importance of Grain Size and Frequency-Dependent Mean Free Paths. *Nano Lett.* **2011**, *11* (6), 2206–2213.

(15) Snyder, G. J.; Toberer, E. S. Complex Thermoelectric Materials. *Nat. Mater.* **2008**, *7* (2), 105–114.

(16) Bux, S. K.; Blair, R. G.; Gogna, P. K.; Lee, H.; Chen, G.; Dresselhaus, M. S.; Kaner, R. B.; Fleurial, J. P. Nanostructured Bulk Silicon as an Effective Thermoelectric Material. *Adv. Funct. Mater.* **2009**, *19* (15), 2445–2452.

(17) Barbagiovanni, E. G.; Lockwood, D. J.; Simpson, P. J.; Goncharova, L. V. Quantum Confinement in Si and Ge Nanostructures: Theory and Experiment. *Appl. Phys. Rev.* **2014**, *1* (1), 011302.

(18) Li, C.; Wang, F.; Yu, J. C. Semiconductor/Biomolecular Composites for Solar Energy Applications. *Energy Environ. Sci.* **2011**, *4* (1), 100–113.

(19) Hoffman, M.; Veinot, J. G. C. Understanding the Formation of Elemental Germanium by Thermolysis of Sol-Gel Derived Organogermanium Oxide Polymers. *Chem. Mater.* **2012**, *24* (7), 1283–1291.

(20) Codoluto, S. C.; Baumgardner, W. J.; Hanrath, T. Fundamental Aspects of Nucleation and Growth in the Solution-Phase Synthesis of Germanium Nanocrystals. *CrystEngComm* **2010**, *12* (10), 2903–2909.

(21) Satyala, N.; Tahmasbi Rad, A.; Zamanipour, Z.; Norouzzadeh, P.; Krasinski, J. S.; Tayebi, L.; Vashaee, D. Influence of Germanium Nano-Inclusions on the Thermoelectric Power Factor of Bulk Bismuth Telluride Alloy. *J. Appl. Phys.* **2014**, *115* (20), 204308.

(22) Fan, J.; Chu, P. K. Group IV Nanoparticles: Synthesis, Properties, and Biological Applications. *Small* **2010**, *6* (19), 2080–2098.

(23) Shirahata, N.; Hirakawa, D.; Masuda, Y.; Sakka, Y. Size-Dependent Color Tuning of Efficiently Luminescent Germanium Nanoparticles. *Langmuir* **2013**, *29* (24), 7401–7410.

(24) Prabakar, S.; Shiohara, A.; Hanada, S.; Fujioka, K.; Yamamoto, K.; Tilley, R. D. Size Controlled Synthesis of Germanium Nanocrystals by Hydride Reducing Agents and Their Biological Applications. *Chem. Mater.* **2010**, *22* (2), 482–486.

(25) Ge, S.; Jiang, K.; Lu, X.; Chen, Y.; Wang, R.; Fan, S. Orientation-Controlled Growth of Single-Crystal Silicon-Nanowire Arrays. *Adv. Mater.* **2005**, *17* (1), 56–61.

(26) Heath, J. R.; Shiang, J. J.; Alivisatos, A. P. Germanium Quantum Dots: Optical Properties and Synthesis. *J. Chem. Phys.* **1994**, *101* (2), 1607–1615.

(27) Lu, X.; Korgel, B. A.; Johnston, K. P. High Yield of Germanium Nanocrystals Synthesized from Germanium Diiodide in Solution. *Chem. Mater.* **2005**, *17* (25), 6479–6485.

(28) Bernard, A.; Zhang, K.; Larson, D.; Tabatabaei, K.; Kauzlarich, S. M. Solvent Effects on Growth, Crystallinity, and Surface Bonding of Ge Nanoparticles. *Inorg. Chem.* **2018**, *57* (9), 5299–5306.

(29) Gerion, D.; Zaitseva, N.; Saw, C.; Casula, M. F.; Fakra, S.; Van Buuren, T.; Galli, G. Solution Synthesis of Germanium Nanocrystals: Success and Open Challenges. *Nano Lett.* **2004**, *4* (4), 597–602.

(30) Lu, X.; Ziegler, K. J.; Ghezelbash, A.; Johnston, K. P.; Korgel, B. A. Synthesis of Germanium Nanocrystals in High Temperature Supercritical Fluid Solvents. *Nano Lett.* **2004**, *4* (5), 969–974.

(31) Myung, N.; Lu, X.; Johnston, K. P.; Bard, A. J. Electrogenerated Chemiluminescence of Ge Nanocrystals. *Nano Lett.* **2004**, *4* (1), 183–185.

(32) Gerung, H.; Bunge, S. D.; Boyle, T. J.; Brinker, C. J.; Han, S. M. Anhydrous Solution Synthesis of Germanium Nanocrystals from the Germanium(II) Precursor Ge[N(SiMe3)2]2. *Chem. Commun.* **2005**, No. 14, 1914–1916.

(33) Lee, D. C.; Pietryga, J. M.; Robel, I.; Werder, D. J.; Schaller, R. D.; Klimov, V. I. Colloidal Synthesis of Infrared-Emitting Germanium Nanocrystals. *J. Am. Chem. Soc.* **2009**, *131* (10), 3436–3437.

(34) Vaughn, D. D.; Bondi, J. F.; Schaak, R. E. Colloidal Synthesis of Air-Stable Crystalline Germanium Nanoparticles with Tunable Sizes and Shapes. *Chem. Mater.* **2010**, *22* (22), 6103–6108.

(35) Prabakar, S.; Shiohara, A.; Hanada, S.; Fujioka, K.; Yamamoto, K.; Tilley, R. D. Size Controlled Synthesis of Germanium Nanocrystals by Hydride Reducing Agents and Their Biological Applications. *Chem. Mater.* **2010**, *22* (2), 482–486.

(36) Johnson, O. H. Germanium and Its Inorganic Compounds. *Chem. Rev.* **1952**, *51* (3), 431–469.

(37) Taylor, B. R.; Kauzlarich, S. M.; Delgado, G. R.; Lee, H. W. H. Solution Synthesis and Characterization of Quantum Confined Ge Nanoparticles. *Chem. Mater.* **1999**, *11* (9), 2493–2500.

(38) Wang, W.; Huang, J.; Ren, Z. Synthesis of Germanium Nanocubes by a Low-Temperature Inverse Micelle Solvothermal Technique. *Langmuir* **2005**, *21* (2), 751–754.

(39) Wu, J.; Sun, Y.; Zou, R.; Song, G.; Chen, Z.; Wang, C.; Hu, J. One-Step Aqueous Solution Synthesis of Ge Nanocrystals from GeO2 Powders. *CrystEngComm* **2011**, *13*, 3674–3677.

(40) Warner, J. H. Solution-Phase Synthesis of Germanium Nanoclusters Using Sulfur. *Nanotechnology* **2006**, *17* (22), 5613–5619.

(41) Ha, E.; Liu, W.; Wang, L.; Man, H. W.; Hu, L.; Tsang, S. C. E.; Chan, C. T. L.; Kwok, W. M.; Lee, L. Y. S.; Wong, K. Y. Cu2ZnSnS4/MoS2-Reduced Graphene Oxide Heterostructure: Nanoscale Interfacial Contact and Enhanced Photocatalytic Hydrogen Generation. *Sci. Rep.* **2017**, *7*, 39411.

(42) Özel, F.; Sarilmaz, A.; Istanbullu, B.; Aljabour, A.; Kuş, M.; Sönmezoğlu, S. Penternary Chalcogenides Nanocrystals as Catalytic Materials for Efficient Counter Electrodes in Dye-Synthesized Solar Cells. *Sci. Rep.* **2016**, *6*, 29207.

(43) Martin, T. R.; Mazzio, K. A.; Hillhouse, H. W.; Luscombe, C. K. Sulfur Copolymer for the Direct Synthesis of Ligand-Free CdS Nanoparticles. *Chem. Commun.* **2015**, *51* (56), 11244–11247.

(44) Schneider, C. A.; Rasband, W. S.; Eliceiri, K. W. NIH Image to ImageJ: 25 Years of Image Analysis. *Nat. Methods* **2012**, *9* (7), 671–675.

(45) Sear, R. P. Nucleation: Theory and Applications to Protein Solutions and Colloidal Suspensions. *J. Phys. Condens. Matter* **2007**, *19* (3), 033101.

(46) Peng, Z. A.; Peng, X. Nearly Monodisperse and Shape-Controlled CdSe Nanocrystals via Alternative Routes: Nucleation and Growth. *J. Am. Chem. Soc.* **2002**, *124* (13), 3343–3353.

(47) De Mello Donegá, C.; Liljeroth, P.; Vanmaekelbergh, D. Physicochemical Evaluation of the Hot-Injection Method, a Synthesis Route for Monodisperse Nanocrystals. *Small* **2005**, *1* (12), 1152–1162.

(48) García, N. A.; Register, R. A.; Vega, D. A.; Gómez, L. R. Crystallization Dynamics on Curved Surfaces. *Phys. Rev. E* **2013**, *88* (1), 012306.

(49) Thomson, W. On the Equilibrium of Vapour at a Curved Surface of Liquid. *Proc. R. Soc. Edinburgh* **1872**, *7* (282), 63–68.

(50) Corsini, N. R. C.; Zhang, Y.; Little, W. R.; Karatutlu, A.; Ersoy, O.; Haynes, P. D.; Molteni, C.; Hine, N. D. M.; Hernandez, I.; Gonzalez, J. Pressure-Induced Amorphization and a New High Density Amorphous Metallic Phase in Matrix-Free Ge Nanoparticles. *Nano Lett.* **2015**, *15* (11), 7334–7340.

(51) Carim, A. I.; Collins, S. M.; Foley, J. M.; Maldonado, S. Benchtop Electrochemical Liquid-Liquid-Solid Growth of Nanostructured Crystalline Germanium. *J. Am. Chem. Soc.* **2011**, *133* (34), 13292–13295.

(52) Andreev, B. A.; Gavrilenko, L. V.; Drozdov, Y. N.; Yunin, P. A.; Pryakhin, D. A.; Mochalov, L. A.; Sennikov, P. G.; Bulkin, P.; Roca I Cabarrocas, P. Raman Spectra of Amorphous Isotope-Enriched 74Ge with Low-Strained Ge Nanocrystals. *Thin Solid Films* **2014**, *552*, 46–49.

(53) Deb, S. K.; Dong, J.; Hubert, H.; McMillan, P. F.; Sankey, O. F. Raman Spectra of the Hexagonal and Cubic (Spinel) Forms of Ge3N4: An Experimental and Theoretical Study. *Solid State Commun.* **2000**, *114* (3), 137–142.

(54) Soignard, E.; McMillan, P. P.; Leinenweber, K. Solid Solutions

and Ternary Compound Formation among Ge3N 4-Si3N4 Nitride Spinels Synthesized at High Pressure and High Temperature. *Chem. Mater.* **2004**, *16* (25), 5344–5349.

(55) MacLachlan, M. J.; Petrov, S.; Bedard, R. L.; Manners, I.; Ozin, G. A. Synthesis and Crystal Structure of δ-GeS2, the First Germanium Sulfide with an Expanded Framework Structure. *Angew. Chemie - Int. Ed.* **1998**, *37* (15), 2075–2079.

(56) Thomson, J. W.; Nagashima, K.; MacDonald, P. M.; Ozin, G. A. From Sulfur-Amine Solutions to Metal Sulfide Nanocrystals: Peering into the Oleylamine-Sulfur Black Box. *J. Am. Chem. Soc.* **2011**, *133* (13), 5036–5041.

(57) Ghosh, P.; Katare, S.; Patkar, P.; Caruthers, J. M.; Venkatasubramanian, V.; Walker, K. A. Sulfur Vulcanization of Natural Rubber for Benzothiazole Accelerated Formulations: From Reaction Mechanisms to a Rational Kinetic Model. *Rubber Chem. Technol.* **2003**, *76* (3), 592–693.

(58) Lewis, W. K.; Squires, L.; Nutting, R. D. Mechanism of Rubber Vulcanization with Sulfur. *Ind. Eng. Chem.* **1937**, *29* (10), 1135–1144.

(59) Kim, E. T.; Chung, W. J.; Lim, J.; Johe, P.; Glass, R. S.; Pyun, J.; Char, K. One-Pot Synthesis of PbS NP/Sulfur-Oleylamine Copolymer Nanocomposites via the Copolymerization of Elemental Sulfur with Oleylamine. *Polym. Chem.* **2014**, *5* (11), 3617–3623.

(60) Grigorovici, R.; Mănăilă, R. Structural Model for Amorphous Germanium Layers. *Thin Solid Films* **1968**, *1* (5), 343–352.

(61) Ruddy, D. A.; Johnson, J. C.; Smith, E. R.; Neale, N. R. Size and Bandgap Control in the Solution-Phase Synthesis of near-Infrared-Emitting Germanium Nanocrystals. *ACS Nano* **2010**, *4* (12), 7459–7466.

(62) Mayer, H. P.; Rapsomanikis, S. Chemical Methylation of Germanium(II) in Model Aqueous Solutions. *Appl. Organomet. Chem.* **1992**, *6* (2), 173–178.

(63) Auer, S.; Frenkel, D. Suppression of Crystal Nucleation in Polydisperse Colloids Due to Increase of the Surface Free Energy. *Nature* **2001**, *413*, 711–713.

(64) Anderson, V. J.; Lekkerkerker, H. N. W. Insights into Phase Transition Kinetics from Colloid Science. *Nature* **2002**, *416*, 811–815.

SYNOPSIS TOC This work details the control of germanium nanoparticle size and crystallinity via colloidal synthesis from benign reagents. We demonstrate that crystalline particles can be formed with saturated long-chain aliphatic amines as solvent, whereas amorphous particles are formed with the addition of a single double bond on the carbon chain. We propose a complete reaction mechanism that can describe these results, and go further to discuss the details of kinetic control.